# Misfit paradox on nucleation potency of MgO and $MgAl_2O_4$ for Al

D. Zhang[1], L. Wang[1], M. Xia[1*], N. Hari Babu[2], J.G. Li[1]

[1] School of Materials Science and Engineering, Shanghai Jiao Tong University, Shanghai, China, 200240

[2] BCAST, Brunel University London, London, UK, UB8 3PH

## ABSTRACT

MgO and $MgAl_2O_4$ are believed to be effective heterogeneous nuclei for Al based alloys due to their small lattice misfits with Al. However, there is a strong evidence to suggest that liquid Al react with MgO and $MgAl_2O_4$ phases but the heterogeneous nucleation behavior of such phases is rarely discussed. In order to identify the nucleation mechanism of Al, under the interference of the chemical reaction, the heterogeneous nucleation process is systematically investigated through thermal analysis and high resolution transmission electron microscopy (HRTEM). The observed multi-nucleation interfaces (Al/MgO, Al/$MgAl_2O_4$ and Al/$Al_2O_3$) and scattered experimental undercooling data indicate an independent multi-phase nucleation process in these systems.

**Keywords**: Aluminum, Heterogeneous nucleation, Single crystal substrate, Interfaces.

[*] Corresponding author: mingxu.xia@sjtu.edu.cn，Tel/Fax: +86-21-54744246

## 1. Introduction

According to classical nucleation theory (CNT), nucleation potency of the heterogeneous particles is believed to be related with the interfacial energy between the particle and newly formed crystal [1] from the melt, which in turn depends on the similarity of the lattice structures of these two solids at the interface [2]. MgO and $MgAl_2O_4$ are common oxides formed during preparation and remelting processes of Al-Mg alloys. Both of them have the similar lattice structure (Face-Centered Cubic, FCC) [3] and small lattice misfit with Al ($f_{Al/MgO}$=3.12% and $f_{Al/MgAl_2O_4}$=1.11%) [4, 5].

Thus, MgO and $MgAl_2O_4$ are believed to be perfect catalyzers for the nucleation of liquid Al [6]. However, a few researches [7-11] reported that liquid Al will react with MgO substrates at a high temperature. In that case, the nucleation behavior will be affect by the reaction products. The interaction of molten Al with MgO was has been discussed in the frame of wetting behavior of MgO with liquid Al, rather than nucleation mechanism point of view. Among these researches, Mcevoy et al. [11] reported that the reaction product of molten Al with MgO was spinel ($MgAl_2O_4$). Fujii and Nakae [10] identified the presence of $Al_2O_3$ oxide at the interface between MgO and liquid Al. Most recently, Morgiel [12] clarified that the spinel was an intermediate product and α -$Al_2O_3$ was a final product of the reaction. Thus, MgO, $MgAl_2O_4$ and $Al_2O_3$ all could be potential nucleation agents when liquid Al solidified on MgO and $MgAl_2O_4$ substrates. In this paper, in order to clarify the nucleation mechanism of formation of Al nuclei on MgO and $MgAl_2O_4$ phases, nucleation interfaces have been systematically investigated using thermal analysis and high resolution transmission electron microscopy (HRTEM). The results are discussed based on Turnbull's misfit theory [2].

## 2. Experimental

In order to ensure the nucleation was triggered by the assigned surface, single crystal MgO and $MgAl_2O_4$ substrates (5 mm × 5 mm × 0.5 mm in dimensions) with less than 0.5 nm surface roughness were used as heterogeneous nucleation substrates. Substrate wafers were commercially obtained with (100), (110), (111) terminated planes. High purity Al (>99.999wt%) was selected as nucleating substance and the melt was cooled on the selective terminated planes of MgO and $MgAl_2O_4$ substrate from 1373(1300?) K in high vacuum chamber with cooling rate of 20 K/s. The cooling curve was recorded by infrared pyrometer [13]. In order to create sufficient chemical reaction

layer for HRTEM study, the liquid Al was soaked at 1300K for 30 seconds. By that time, the wetting of Al on substrate was proved at a quasi-equilibrium stage [14]. Each thermal test cycle was repeated at least 5 times following the same test procedure to ensure the reliability of the measured results. The preferred growth orientations of new Al crystal were detected by X-ray diffraction (XRD) using XRD Ultima IV equipment. Nucleation interface was investigated along vertical section, and surface of the substrate was analyzed after new Al crystal was chemically removed from the substrate using 15 wt% NaOH distilled-water solution. Microstructural observation was carried out under a low vacuum scanning electron microscope (LV-SEM, Type: FEI Nova NanoSEM 230) equipped with an electron dispersive X-ray (EDX) spectrometer. The phase composition and crystal orientation of nucleation surface were identified by XRD through the same XRD Ultima IV. For high-resolution analytical electron microscopy, thin samples were fabricated under a focused ion beam (FIB) SEM (FEI Helios 600i System) equipped with dual (ion and electron) beam and an EDX system. The transmission electron microscopy (TEM) and high resolution TEM (HRTEM) analyses were conducted on a Tecnai G2s-Twin TEM instrument operated at an accelerating voltage of 200kv.

## 3. Results

### 3.1 Al crystal on MgO and $MgAl_2O_4$ single crystal substrates

According to the XRD patterns of the nucleated surfaces in Fig. 1, the orientations of MgO substrates do not have remarkable influence on the preferred growth orientations of nucleated Al crystal. The natural growth orientation of Al (111) was

still the most preferred orientation of newly formed crystal despite the heterogeneous nuclei facilitated by the substrates terminated with various crystal planes. However, the same substrate, such as $MgAl_2O_4$, can also trigger different preferred orientations of new crystal (e.g., Al (111) and Al (311) on $MgAl_2O_4$ (111); Al (220) and Al (311) on $MgAl_2O_4$ (110); Al (111) and Al (200) on $MgAl_2O_4$ (100)). The varied preferred growth orientations of Al crystal on various $MgAl_2O_4$ substrates indicates that the orientations of substrates are able to affect nucleation process to some extent, although it is not decisive factor.

Considering the detected growth direction of new Al in Fig. 1, the matching plane of new crystal with the substrate is no longer the natural low index planes as defined in Bramfitt's equation [15]. Thus, the calculation of the theoretical lattice misfit between new Al crystals and various substrates is modified as,

$$f_{(hkl)_n}^{(hkl)_s} = \sum_{i=1}^{3} \frac{\left| d_{[uvw]_s^i} \cos\theta - d_{[uvw]_n^i} \right|}{3 d_{[uvw]_n^i}} \times 100\% \quad (1)$$

where *$(hkl)_s$ is the terminated plane of single crystal substrate*, which was supposed to be the nucleation surface, $[uvw]_s$ is the low index direction of the terminate plane, $(hkl)_n$ is the *preferred growth plane of the new crystalline phase based on XRD results*, $[uvw]_n$ is the low index direction of the plane, $d_{[uvw]s}$ is the atomic separation along direction $[uvw]_s$, $d_{[uvw]n}$ is the atomic separation along direction $[uvw]_n$, $\theta$ is the angle between $[uvw]_s$ and $[uvw]_n$. Taking into account the lattice expansion at high temperature [16], lattice parameter of Al, MgO and $MgAl_2O_4$ are 0.411nm, 0.424nm and 0.813nm respectively [3,5]. The lattice misfits between nucleated Al crystal and

(100), (110), (111) MgO and $MgAl_2O_4$ single crystal substrates are shown in Table 1. Turnbull [4] and Bramfitt [15] proposed a distinct relationship between undercooling and lattice misfit (*f*). The smaller lattice misfit leads to a smaller undercooling, and indicating higher nucleation potency of the substrate. Combing the calculated lattice misfit results in Table 1 and measured undercooling in our experiments, a misfit-undercooling ($f$-$\Delta T$) diagram is illustrated in Fig. 2. The illustration shows a relatively scattered undercooling range between 15 K and 30 K, regardless of the orientation and material of the substrate. It means both lattice misfit and substrate material had limited effect on the nucleation of Al. Apparently, the results are not in agreement with Turnbull's theory. It is known that [7-11], there exists a chemical reaction between liquid Al and MgO substrate and this disagreement is thought primarily due to the presence of reaction product phases in the vicinity of MgO substrate and these may influence the measured undercooling values.

**3.2** Reaction products at Al/MgO and Al/$MgAl_2O_4$ interfaces

In order to verify possible reaction products at the interface, typical SEM analysis on both nucleation interface (i.e. interface between newly formed Al crystal and MgO or $MgAl_2O_4$ substrate) and nucleation surface (i.e, Top surface of newly formed Al crystal on the MgO or $MgAl_2O_4$ substrate) is conducted and the images are presented in Fig. 3 together with EDX mapping results. A reaction layer with tens of microns thickness is observed to form on the surface of the substrate as fully developed dendrite-like structure beneath the interface??. Above the reaction layer, polycrystalline Al layer is observed. Below the reaction layer, substrate is observed to

corrode due to chemical reaction. EDX mappings on both vertical section and nucleation surface indicate that the reaction layer contained Al and O, which is consistent with previous reports [7-10]. At the reaction layer surface (i.e. the nucleation surface) a sharp elemental transition between dendrites and non-reaction surface region is detected. Non-reaction area consists of a higher Mg content, while in dendritic area the Mg content vanished due to the evaporation during the interfacial reaction, as explained in Ref. [12].

The phase composition of the nucleation surface was further verified through XRD (Fig. 4). Combining EDX analysis and XRD patterns, the Al-O dendrites layer on the nucleation surface is confirmed to be $Al_2O_3$ phase at both Al/MgO and Al/$MgAl_2O_4$ interfaces. Apart from $Al_2O_3$, a traces of $MgAl_2O_4$ phase is also detected on MgO substrates, which indicates an intermediate chemical reaction existing at Al/MgO interface as reported in Ref. [11]. The intermediate reaction product $MgAl_2O_4$ would further react with Al forming $Al_2O_3$ and Mg, which evaporates. The whole reaction process was discussed by Morgiel et al Ref.[12] in detail showing $MgAl_2O_4$ is the first stage product of the reaction between molten Al and MgO at high temperature. Liquid Al would then penetrate the gaps between $Al_2O_3$ dendrites and these channels are in direct contact with the substrates. Although $Al_2O_3$ was the final reaction product on single crystal substrate, XRD pattern on the exposed surface of $Al_2O_3$ didn't show any preferred orientation as newly formed Al crystal did. High magnification observation on the surface of $Al_2O_3$ shows a corroded surface which may scattered the exposed orientations of $Al_2O_3$.

**3.3** Nucleation interfaces under TEM

Since original substrates (MgO and $MgAl_2O_4$) and reaction product $Al_2O_3$ all are in contact with Al and are able to trigger the nucleation of liquid Al, the interfaces between Al and these oxides were further investigated in detail to identify the real nucleation interface of the systems. Typical TEM samples were sectioned from the interfaces between both solidified Al and original substrate or the reaction layer using FIB technique. Fig. 5a illustrates the bright-filed (BF) image of a TEM sample sectioned from the upper reaction interface of Al/MgO system. Selected area electron diffraction (SAED) patterns (Fig. 5c) also indicates that the reaction layer is $Al_2O_3$, which has a Hexagonal Close-Packed (HCP) structure with the lattice parameter a=0.476nm [3]. The presence of newly formed $Al_2O_3$ crystals at the intermediate area between Al droplet and MgO substrate, inhibits the direct contact of liquid Al with the original substrate. However, liquid Al would penetrate through the gaps between these $Al_2O_3$ dendrites, as shown in Fig. 3. The details are presented in Fig. 5a and labelled with red arrows.

The lower region of interface between the reaction layer and original MgO substrate is shown in Fig. 6a. SAED pattern from the bright phase (Fig. 6c) indicates that, the bright phase is Al which solidified from the penetrated liquid Al between the gaps of dendritic $Al_2O_3$. The upper region in Fig. 6a is newly formed $Al_2O_3$ (Fig. 6b), while the lower region is the corroded MgO substrate (Fig. 6d). In the case of lower region of interface of Al/$MgAl_2O_4$ reaction layer, as shown in Fig. 6e, liquid Al also penetrated through $Al_2O_3$ layer and contacted $MgAl_2O_4$ substrate directly as identified

in Fig. 6f, g, h.

In both cases, liquid Al has full chance to contact with the three oxide phases. The heterogeneous nucleation process could be trigged by any of them. But whichever the oxide is responsible for the nucleation event, it is important to note that it is not the original exposed surface which triggers the nucleation process. Thus, the correlation between lattice misfit calculation based on crystal planes of original substrates and the measured undercooling shown in Fig.2 is not valid. It should be based on the lattice mismatch between experimentally observed nucleation interfaces, which can be revealed by HRTEM.

3.4 Observed lattice mismatching at the interfaces

The matching planes at the nucleation interface are identified though High resolution TEM analysis on observed Al/MgO, Al/$MgAl_2O_4$ and Al/$Al_2O_3$ interfaces. HRTEM images with corresponding SAED patterns (by fast Fourier transformation) are illustrated in Fig. 7 and 8. Since MgO has the similar lattice structure and lattice parameter with Al [3, 5], the lattice misfit at Al/MgO interface should be small. The orientation relationship (OR) of two matching phases was $(02\bar{2})$[011]Al//$(02\bar{2})$[011]MgO as illustrated in Fig. 7a. Based on SAED patterns in Fig. 7b, the lattice spacing between matching $(1\bar{1}1)_{Al}$ and $(1\bar{1}1)_{MgO}$ is calculated as 0.234 nm and 0.242 nm, respectively. The lattice misfit between $(02\bar{2})_{Al}$ and $(02\bar{2})_{MgO}$ planes is only 3.12% calculated by modified Bramfitt equation [15]. As the lattice spacing of $(1\bar{1}1)_{MgO}$ is slightly larger than $(1\bar{1}1)_{Al}$, an edge dislocation was easily formed at interface along $[21\bar{1}]$ direction.

The HRTEM image and corresponding SAED pattern of Al/$MgAl_2O_4$ interface are shown in Fig. 8 a, b, c. The OR between Al crystal and $MgAl_2O_4$ substrate was $(11\bar{1})[011]Al//(200)[013]MgAl_2O_4$. The misfit between the two matching planes was calculated as about 8.36%, which was larger than that of Al/MgO interface. Based on SAED pattern the lattice spacing of $(1\bar{3}1)_{MgAl_2O_4}$ (0.244 nm) was slightly larger than 0.202 nm of $(200)_{Al}$ at the matching interface along $[2\bar{1}1]_{Al}$ direction. As Fig.8a illustrated, a distorted layer about 1 nm thick was formed between the two matching planes in order to relieve the strain between matching planes. Moreover, a series of periodical dislocations could be observed at the interface along $[2\bar{1}1]_{Al}$ direction which released the lattice strain between two matching planes, $(11\bar{1})_{Al}$ and $(200)_{MgAl_2O_4}$.

HRTEM analysis of the Al/$Al_2O_3$ interface is shown in Fig. 9 a, b, c. The observed OR of matching planes are $(\bar{1}3\bar{3})[011]Al//(0\bar{2}21)[\bar{1}2\bar{1}6]Al_2O_3$. As shown in Fig. 9 a, the lattice spacing of $(10\bar{1}0)_{Al_2O_3}$ was 0.412 nm, nearly twice of 0.234nm for $(11\bar{1})_{Al}$ along $[61\bar{1}]_{Al}$ direction at matching interface. Moreover, the lattice structure of $Al_2O_3$ was HCP structure, different from FCC structure of Al, leading to a large lattice misfit at the interface as 12.93%. Therefore, in order to match $(\bar{1}3\bar{3})_{Al}$ and $(0\bar{2}21)_{Al_2O_3}$ planes, 1-2 coincidence mismatching was introduced along $[61\bar{1}]_{Al}$ direction, which could be observed in Fig. 9 c.

HRTEM analysis on Al/MgO, Al/$MgAl_2O_4$ and Al/$Al_2O_3$ nucleation interfaces indicates that the lattice misfits of the investigating systems ranged so widely from 3.12% to 12.93%. From the HRTEM analysis, it can be seen that the chemical

reaction of Al with MgO and $MgAl_2O_4$ substrates at high temperatures did affect the nucleation of Al on assigned oxide substrates.

## 4. Discussions

### 4.1 Multi nucleation interface leading to scattered undercooling values

In section 3.1, we presented a relatively scattered undercooling range of Al nucleated on various MgO and $MgAl_2O_4$ substrates, which contradicts the predicted parabolic relationship between undercooling and lattice misfit. However, as HRTEM analysis illustrated in Fig. 7, 8 and 9, the initial terminated planes of the substrates are no longer the nucleation surfaces. Alternatively, newly formed $(02\bar{2})_{MgO}$, $(200)_{MgAl_2O_4}$, $(0\bar{2}21)_{Al_2O_3}$ acted as the potential nucleation surfaces. Based on these observed results, the lattice misfit range obtained from HRTEM image analysis is widely varied from 3.12% to 12.93%. According to Turnbull's misfit theory [4], the small misfit will lead to a smaller undercooling, and vice versa. Fig. 10 shows the undercooling data collected from one of our test presenting a large span of the undercooling value from 0 K to 40 K, which is consistent with the obtained misfit values from HRTEM. The small value of the undercooling may be triggered by the nucleation interface with smaller misfit as 3.12%, and the large one by the larger misfit, as concluded by Turnbull [4]. Comparing with this multi substrates triggered nucleation events, the undercooling of levitated liquid drops or the undercooling tested on an inert single crystal substrate [17, 18], which means only one substrate nucleated, has much narrower range. The dispersion of the measured undercooling values is less than 20%. From the comparison, it can be deducted that chemical reaction induced multi

nucleation substrates led to a scattered undercooling values during the test.

The relation between undercooling and lattice misfit can be expressed by Turnbull's parabolic equation [4],

$$\Delta T = \left(\frac{c\times 10^{-1}}{\Delta S_v}\right) f^2 \qquad (2)$$

where c is the elastic modulus of the metal, 72 GPa for pure Al [3] and $\Delta S_v$ is the volume entropy of aluminum, 28.25 $Jmol^{-1}K^{-1}$ [19]. The predicted undercooling (ΔT) variation with misfits (*f*) is plotted in Fig. 11. As illustrated, the parabolic dashed line is the *f*-ΔT fitting relationship curve of Al on substrates with different lattice misfits. According to the *f*-ΔT curve, three undercooling values corresponding to the detected lattice misfits of 3.12%, 8.36%, and 12.93% are expected to be 2.48 K, 17.8 K and 42.6 K, respectively, as shown in Fig. 11. The shadow area is the range of measured undercooling results (0 to 40 K) in our experiment, which covers the predicted undercooling range. It well explains that the scattered experimental undercooling values, between 0 and 40 K, is induced by the nucleation of multi-phases with various misfits. Thus, the newly formed $Al_2O_3$, $MgAl_2O_4$ and MgO, all act as the nucleation substrate leading to a wide undercooling value range.

4.2 Large undercooling induced by "small lattice misfit"

According to conventional theory, smaller misfit means smaller interfacial energy and higher nucleation tendency. Thus, a good matching interface is more effective in triggering the nucleation of new crystal, and a smaller undercooling value should be more expecting. However, as shown in Fig. 10, most of the measured undercooling values are between 15 K and 35 K even though the liquid Al was solidified on low

lattice mismatch substrate of $MgAl_2O_4$.

As mentioned, liquid Al can penetrate into the gaps between $Al_2O_3$ crystals and directly contacts with $MgAl_2O_4$ (MgO) substrate. At the contacting point, liquid would be easily nucleated because of the small lattice misfit. However, these nucleation points on $MgAl_2O_4$ (MgO) substrate could rarely occur due to presence of reaction layer, which diminishes the chances of liquid Al getting in contact with on $MgAl_2O_4$ (MgO) substrates. ~~The temperature signal released by the nucleation event was easily covered by the signal from upper layer~~. Thus, although the original substrates had smaller lattice misfit with Al, the multi-potential nucleation agents in reaction layer would affect the programmed nucleation showing a scattered undercooling values. The detected nucleation events in most of the cases are within the reaction layer, in which $Al_2O_3$ triggers heterogeneous nuclei, leading to a large undercooling value. But in a few cases, the nucleation interfaces of Al/MgO or Al/$MgAl_2O_4$ still can be detected when the reaction layer is thin enough.

## 5. Summary

Due to the chemical reaction between liquid Al and MgO or $MgAl_2O_4$ substrates, the nucleation behavior of Al/MgO and Al/$MgAl_2O_4$ systems is more complicated due to the involved reaction products. Original substrates MgO, $MgAl_2O_4$ and reaction product $Al_2O_3$ are all be able to nucleate Al. The observed nucleation interfaces, Al/MgO, Al/$MgAl_2O_4$ and Al/$Al_2O_3$, have various lattice misfits of 3.12%, 8.36%, and 12.93%, respectively. Owing to the presence of multiple nucleation agents, the detected undercooling is influenced by formation of multi-phase heterogeneous

nucleation interfaces, consequently showing relatively scattered values within a large temperature range from 0 K to 40 K, irrespective of the nature/type of exposed plane of the selected substrates. However, the most of the measured undercooling values lie within a range of 15 K to 30 K, which indicates that heterogeneous nucleation process is dominated by $Al_2O_3$ phase among the three different oxide phases of $Al_2O_3$, MgO and $MgAl_2O_4$.

**Acknowledgements**

The authors are grateful for the useful discussion with Associate Prof. Wenchao Yang, NWPU of China and the financial support from NSFC (No. 51174134, No. 51474148), Shanghai STC (No. 11JC1405900) and NBRPC (No. 2011CB012900).

**Figure captions**

Fig. 1 XRD patterns of new Al crystals on MgO and $MgAl_2O_4$ single crystal substrates with various terminated crystal planes showing that the orientation of substrate is able to affect the preferred growth orientations of newly formed Al crystal to some extent.

Fig. 2 Measured undercooling of Al on MgO and $MgAl_2O_4$ substrates as a function of calculated lattice misfits using Bramfitt method.

Fig. 3 SEM images of Al/MgO nucleation interface. EDX element mappings on

vertical section and nucleation surface revealing that reaction layer is of Al-O phase.

Fig. 4 XRD patterns of typical nucleation surfaces of MgO and MgAl2O4 substrates showing that it is mostly covered by $Al_2O_3$. Negligible $MgAl_2O_4$ was found on MgO substrate.

Fig. 5 (a) Typical TEM image of the upper region of interface showing both newly formed Al crystal and chemical reaction layer. SAED patterns confirm that reactive product is $Al_2O_3$. (b) and (c) shows the recorded SAED patterns for Al and $Al_2O_3$ crystals, respectively. Note that the liquid Al penetrated between $Al_2O_3$ chemical reaction products and solidified.

Fig. 6 Typical TEM images of the lower region of interface between reaction layer and original substrates of (a) MgO and (e) $MgAl_2O_4$. The phases seen in these (a) & (e) micrographs are identified by recording SAED patterns and are labelled. The recorded SAED patterns shown in (b)-(d) and (f)-(h) reconfirms that the reaction layer was $Al_2O_3$ and liquid Al penetrated through the reaction layer contacting with MgO or $MgAl_2O_4$ substrates.

Fig. 7 (a) HRTEM image of Al/MgO interface, (b) the corresponding SAED patterns (by Fast Fourier Transformation) and (c) the indexed patterns corresponding to (b).

Fig. 8 (a) HRTEM image of Al/$MgAl_2O_4$ nucleation interface, (b) the corresponding SAED patterns (by Fast Fourier Transformation) and (c) the indexed patterns corresponding to (b).

Fig. 9 (a) HRTEM image of Al/$Al_2O_3$ nucleation interface, (b) the corresponding SAED patterns and (c) the indexed patterns corresponding to (b).

Fig. 10 Undercooling values of Al nucleated on $MgAl_2O_4$ single crystal substrate collected by pyrometer at each heating cycle showing that the undercooling has a wide range from 0 K to over 40 K and mostly within the range of 15 K to 35 K.

Fig. 11 Misfit-undercooling ($f$-$\Delta T$) fitting curve based on Turnbull's parabolic equation [4] with three predicted undercooling values showing a potential widely ranged undercooling if Al are triggered by $Al_2O_3$, MgO and $MgAl_2O_4$ substrates simultaneously.

Table caption

Table 1 Theoretical lattice misfit ($f$) between Al and MgO single crystal substrate and also between Al and $MgAl_2O_4$ single crystal substrate with different terminated planes

**References**

[1] M. E. Glicksman, W. J. Childs, Nucleation in undercooled liquid tin, Acta Metall. 10(1962)925-933.

[2] H. Fredriksson, U. Åkerlind, Solidification and Crystallization Processing in Metals and Alloys, United Kingdom, 2012.

[3] J. R. Davis, Metals Handbook Desk Edition, 2nd ed., ASM International, Ohio, 1998.

[4] D. Turnbull, B. Vonnegut, Nucleation catalysis, Ind. Eng. Chem. 44(1952)1292-1298.

[5] J. F. Grandfield, D. G. Eskin, I. Bainbridge, Direct-chill Casting of Light Alloys: Science and Technology, New Jersey, 2013.

[6] H. T. Li, Y. Wang, Z. Fan, Mechanisms of enhanced heterogeneous nucleation during solidification in binary Al–Mg alloys, Acta Mater. 60(2012)1528-1537.

[7] D. A. Weirauch, Interfacial phenomena involving liquid metals and solid oxides in the Mg–Al–O system, J. Mater. Res. 3(1988)729-739.

[8] J. Morgiel, N. Sobczak, M. Pomorska, R. Nowak, J. Wojewoda-budka, TEM investigation of phases formed during aluminium wetting of MgO at [100], [110] and [111] orientations, Archive of Metallurgy and materials, 58(20132)497-500.

[9] P. Shen, H. Fuijii, K. Nogi, Effect of substrate crystallographic orientation on wettability and adhesion in several representative systems, J. Mater. Proc. Tech. 155-156(2004)1256-1260.

[10] H. Fujii, H. Nakae, Three wetting phases in the chemically reactive MgO/Al system, ISIJ Int. 30 (1990) 1114–1118.

[11] A.J. Mcevoy, R.H. Wiliams, I.G. Higginbotham, Metal/non-metal interfaces. The wetting of magnesium oxide by aluminium and other metals, J. Mater. Sci. 11(1976) 297–302.

[12] J. Morgiel, N. Sobczak, M. Pomorska, R. Nowak, First stage of reaction of molten Al with MgO substrate, Materials Characterization 103(2015)133-139.

[13] L. Yang, M. Xia, J. G. Li, Epitaxial growth in heterogeneous nucleation of pure aluminum, Mater. Lett. 132(2014)52-54.

[14] P. shen, H. Fujii, T. Matsumoto, K. Nogi, Wetting and reaction of MgO single crystals by molten Al at 1073-1473K, Acta Mater. 52(2004)887-898.

[15]B.L. Bramfitt., The effect of carbide and nitride additions on the heterogeneous nucleation behavior of liquid iron, Metall. Trans., 1(1970)1987-1995.

[16] G. Fiquet, P. Richet, G. Montagnac, High-temperature thermal expansion of lime, periclase, corundum and spinel, Phys. Chem. Minerals 27(1999)103-111.

[17] J. H. Perepezko, M. K. Hoffmeyer, M. P. De Cicco, Analysis of melt undercooling and crystallization kinetics, Metall. Mater. Trans. A 46(2015)4898-4907.

[18] T. Suzuki, J. Inoue, T. Koseki, Solidification of iron and steel on single-crystal oxide, ISIJ Inter. 47(2007)847-852.

[19] P. D. Desai, Thermodynamic properties of aluminum, International Journal of Thermophysics, 8(1987)621-638.

Table 1

| Matching planes | Calculated theoretical lattice misfit $f$ (%) |
|---|---|
| **(100)MgO // (111)Al** | 10.83 |
| **(110)MgO // (111)Al** | 10.00 |
| **(110)MgO // (311)Al** | 14.49 |
| **(111)MgO // (111)Al** | 3.12 |
| **(111)MgO // (220)Al** | 13.87 |
| **(100)$MgAl_2O_4$ // (111)Al** | 12.49 |
| **(110)$MgAl_2O_4$ // (220)Al** | 1.11 |
| **(110)$MgAl_2O_4$ // (311)Al** | 16.01 |
| **(111)$MgAl_2O_4$ // (111)Al** | 1.11 |
| **(111)$MgAl_2O_4$//(311)Al** | 6.20 |

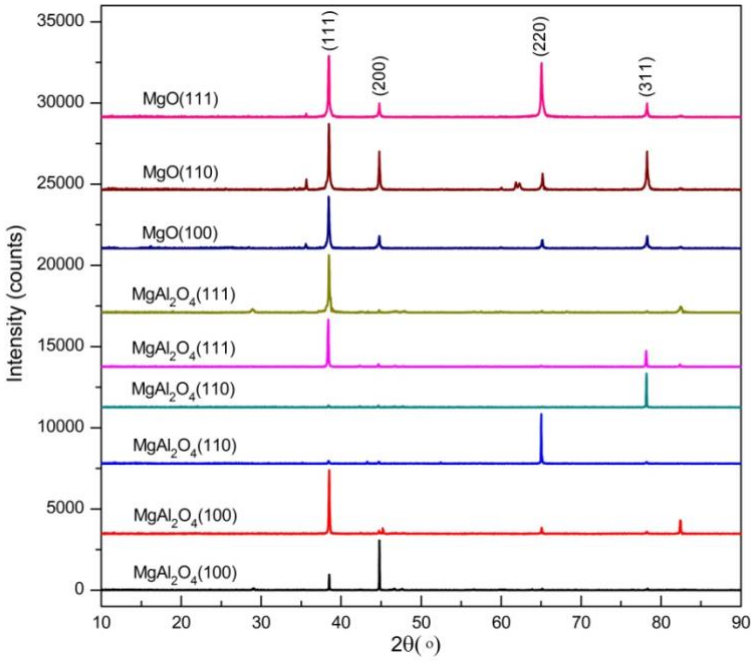
(111)
(200)
(220)
(311)
MgO(111)
MgO(110)
MgO(100)
MgAl2O4(111)
MgAl2O4(111)
MgAl2O4(110)
MgAl2O4(110)
MgAl2O4(100)
MgAl2O4(100)
Intensity (counts)
2θ(o)
35000
30000
25000
20000
15000
10000
5000
0
10
20
30
40
50
60
70
80
90

Fig. 1

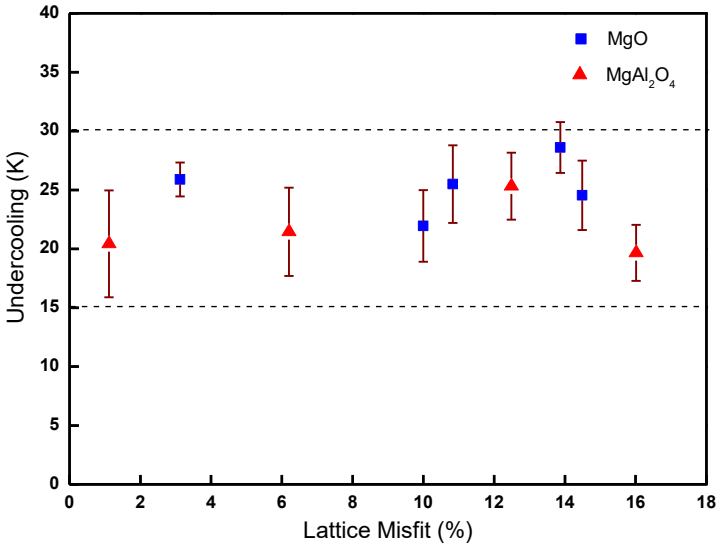
MgO
MgAl2O4
Undercooling (K)
Lattice Misfit (%)
0
5
10
15
20
25
30
35
40
0
2
4
6
8
10
12
14
16
18

Fig. 2

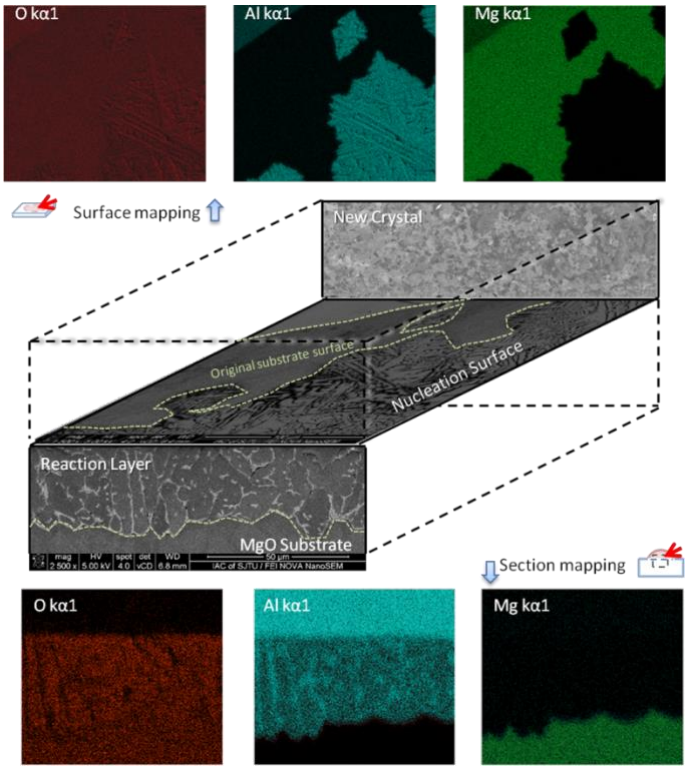
O kα1
Al kα1
Mg kα1
Surface mapping
New Crystal
Original substrate surface
Nucleation Surface
Reaction Layer
MgO Substrate
Section mapping
O kα1
Al kα1
Mg kα1

Fig. 3

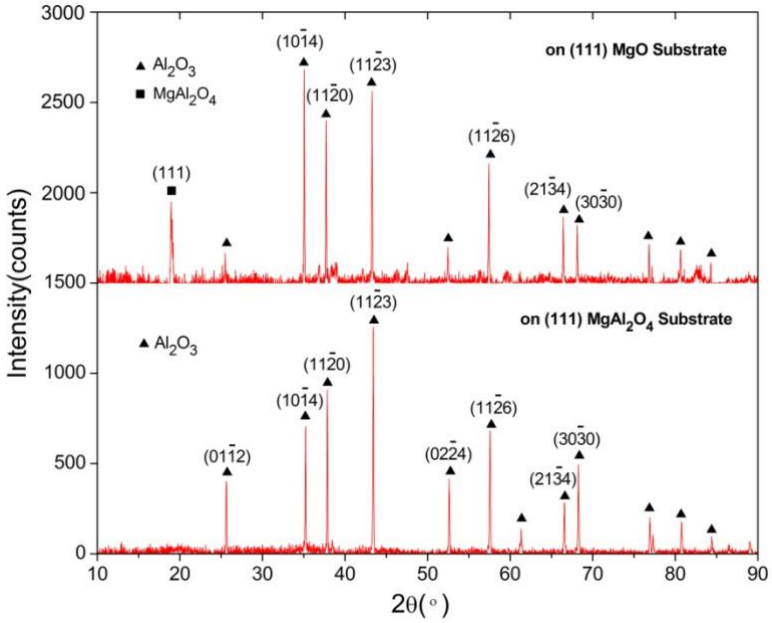
on (111) MgO Substrate
▲ $Al_2O_3$
■ $MgAl_2O_4$
(111)
$(10\bar{1}4)$
$(11\bar{2}0)$
$(11\bar{2}3)$
$(11\bar{2}6)$
$(21\bar{3}4)$
$(30\bar{3}0)$
on (111) $MgAl_2O_4$ Substrate
▲ $Al_2O_3$
$(01\bar{1}2)$
$(10\bar{1}4)$
$(11\bar{2}0)$
$(11\bar{2}3)$
$(02\bar{2}4)$
$(11\bar{2}6)$
$(21\bar{3}4)$
$(30\bar{3}0)$
Intensity(counts)
2θ(°)
0
500
1000
1500
2000
2500
3000
10
20
30
40
50
60
70
80
90

Fig. 4

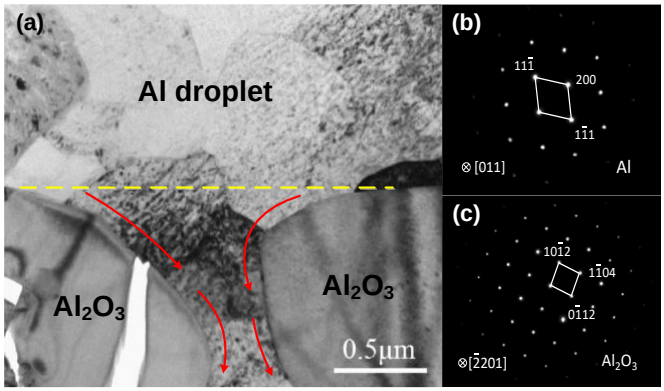
(a)
Al droplet
$Al_2O_3$
$Al_2O_3$
0.5μm
(b)
$11\bar{1}$
200
$1\bar{1}1$
⊗ [011]
Al
(c)
$10\bar{1}2$
$1\bar{1}04$
$01\bar{1}2$
⊗[$\bar{2}$201]
$Al_2O_3$

Fig. 5

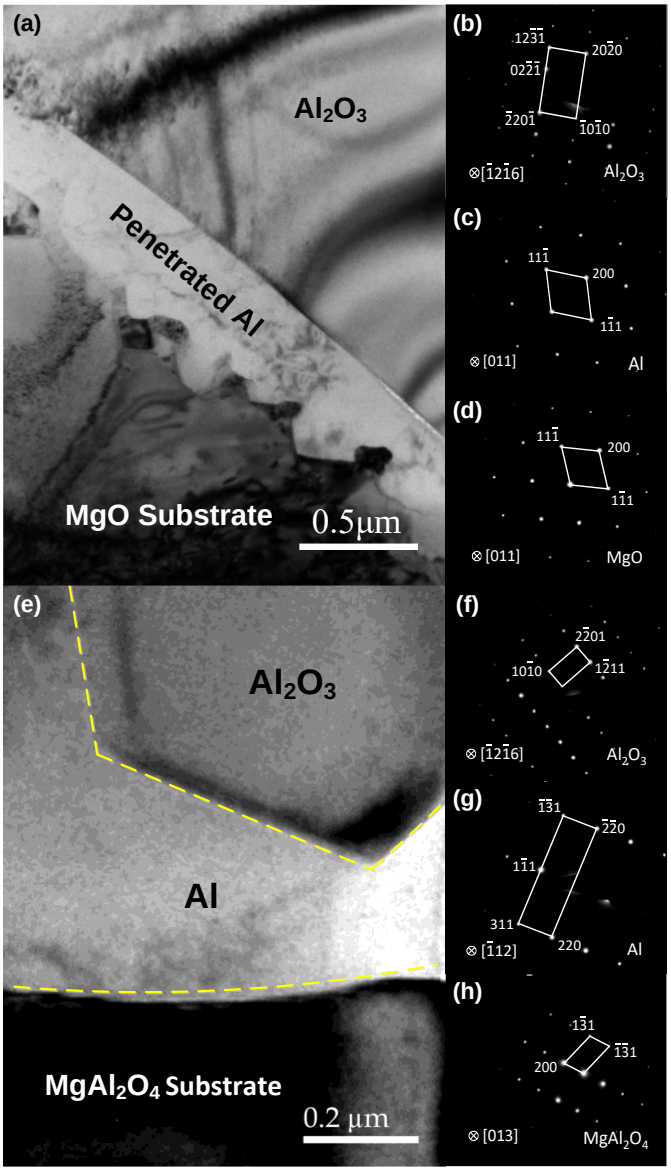
(a)
$Al_2O_3$
Penetrated Al
MgO Substrate
0.5μm
(b)
$\otimes[\bar{1}2\bar{1}6]$
$Al_2O_3$
(c)
$\otimes$ [011]
Al
(d)
$\otimes$ [011]
MgO
(e)
$Al_2O_3$
Al
$MgAl_2O_4$ Substrate
0.2 μm
(f)
$\otimes[\bar{1}2\bar{1}6]$
$Al_2O_3$
(g)
$\otimes[\bar{1}12]$
Al
(h)
$\otimes$ [013]
$MgAl_2O_4$

Fig. 6

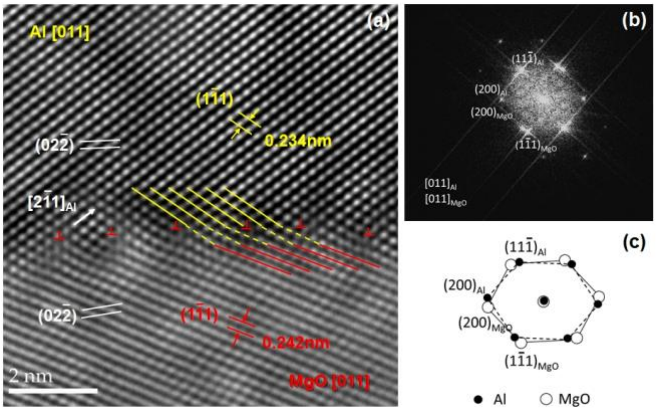
Al [011]
(a)
(1$\bar{1}$1)
0.234nm
(02$\bar{2}$)
[2$\bar{1}$1]$_{Al}$
(02$\bar{2}$)
(1$\bar{1}$1)
0.242nm
2 nm
MgO [011]
(b)
(11$\bar{1}$)$_{Al}$
(200)$_{Al}$
(200)$_{MgO}$
(1$\bar{1}$1)$_{MgO}$
[011]$_{Al}$
[011]$_{MgO}$
(c)
(11$\bar{1}$)$_{Al}$
(200)$_{Al}$
(200)$_{MgO}$
(1$\bar{1}$1)$_{MgO}$
Al
MgO

Fig. 7

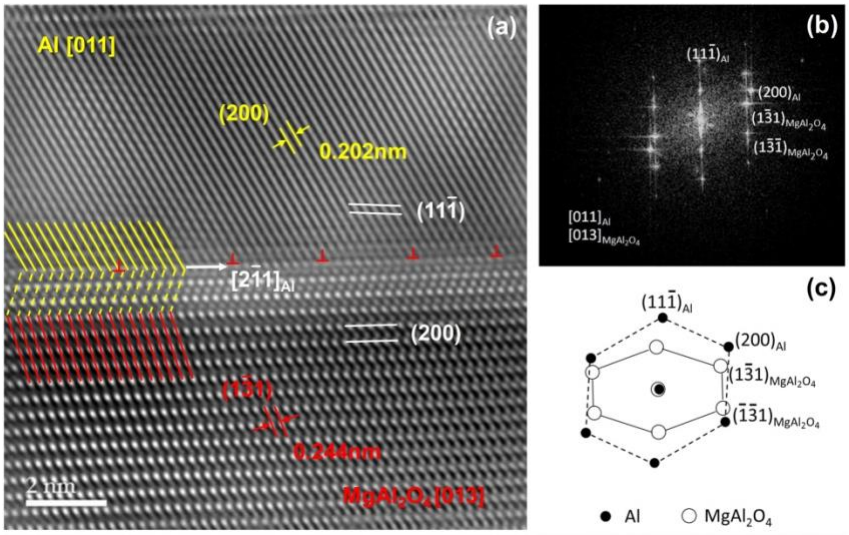
(a)
Al [011]
(200)
0.202nm
(11$\bar{1}$)
[2$\bar{1}$1]$_{Al}$
(200)
(13$\bar{1}$)
0.244nm
2 nm
MgAl$_2$O$_4$[013]
(b)
(11$\bar{1}$)$_{Al}$
(200)$_{Al}$
(13$\bar{1}$)$_{MgAl_2O_4}$
(13$\bar{1}$)$_{MgAl_2O_4}$
[011]$_{Al}$
[013]$_{MgAl_2O_4}$
(c)
(11$\bar{1}$)$_{Al}$
(200)$_{Al}$
(1$\bar{3}$1)$_{MgAl_2O_4}$
($\bar{1}\bar{3}$1)$_{MgAl_2O_4}$
Al
MgAl$_2$O$_4$

Fig. 8

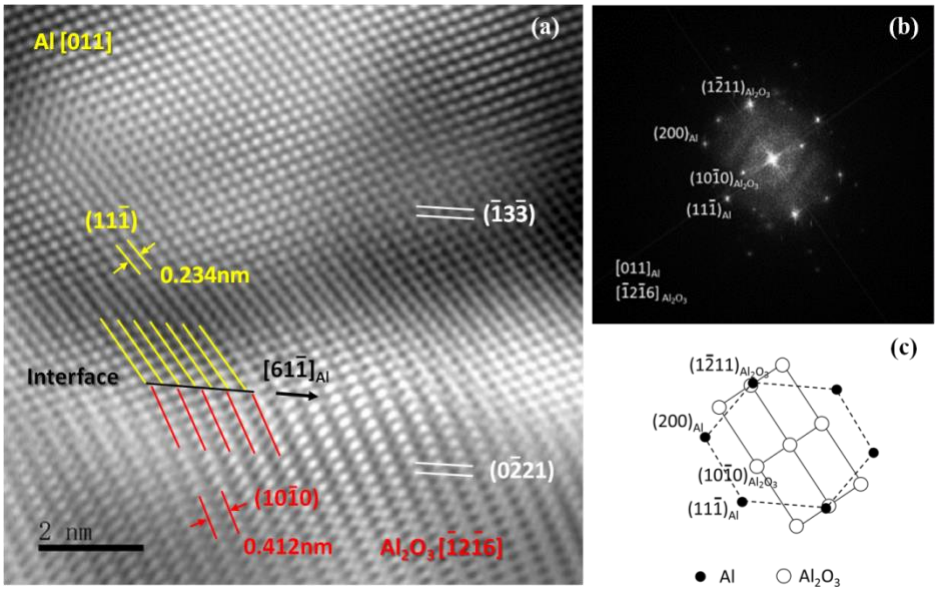
(a)
Al [011]
(11$\bar{1}$)
0.234nm
($\bar{1}\bar{3}\bar{3}$)
Interface
[6$\bar{1}\bar{1}$]$_{Al}$
(0$\bar{2}$21)
(10$\bar{1}$0)
0.412nm
$Al_2O_3$[$\bar{1}$2$\bar{1}$6]
2 nm
(b)
(1$\bar{2}$11)$_{Al_2O_3}$
(200)$_{Al}$
(10$\bar{1}$0)$_{Al_2O_3}$
(11$\bar{1}$)$_{Al}$
[011]$_{Al}$
[$\bar{1}$2$\bar{1}$6]$_{Al_2O_3}$
(c)
(1$\bar{2}$11)$_{Al_2O_3}$
(200)$_{Al}$
(10$\bar{1}$0)$_{Al_2O_3}$
(11$\bar{1}$)$_{Al}$
Al
$Al_2O_3$

Fig. 9

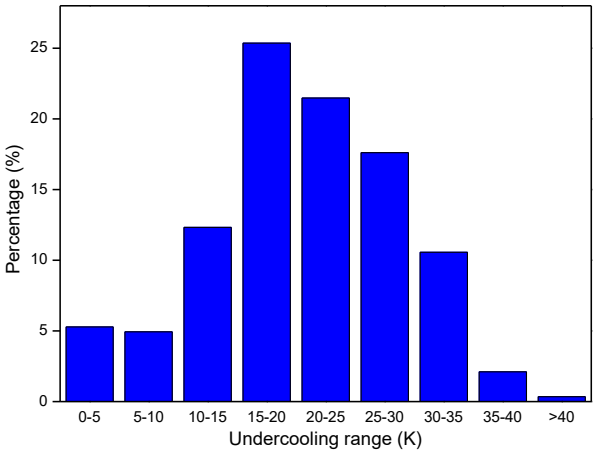
Percentage (%)
0
5
10
15
20
25
0-5
5-10
10-15
15-20
20-25
25-30
30-35
35-40
>40
Undercooling range (K)

Fig. 10

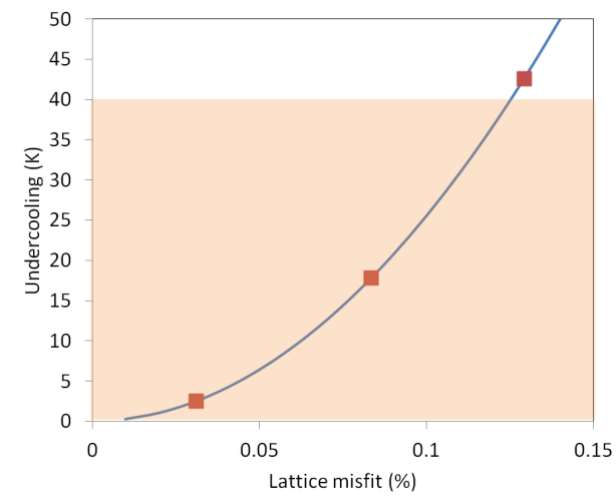
50
45
40
35
30
25
20
15
10
5
0
Undercooling (K)
0
0.05
0.1
0.15
Lattice misfit (%)

Fig. 11